

The 266-nm ultraviolet-beam generation of all-fiberized super-large-mode-area narrow-linewidth nanosecond amplifier with tunable pulse width and repetition rate

Shun Li(李舜), Ping-Xue Li(李平雪), Min Yang(杨敏), Ke-Xin Yu(于可新), Yun-Chen Zhu(朱云晨), Xue-Yan Dong(董雪岩), and Chuan-Fei Yao(姚传飞)

Citation: Chin. Phys. B, 2022, 31 (**3**): 034207. DOI: 10.1088/1674-1056/ac192b
Journal homepage: http://cpb.iphy.ac.cn; http://iopscience.iop.org/cpb

What follows is a list of articles you may be interested in

High-sensitive terahertz detection by parametric up-conversion using nanosecond pulsed laser

Yuye Wang(王与烨), Gang Nie(聂港), Changhao Hu(胡常灏), Kai Chen(陈锴), Chao Yan(闫超), Bin Wu(吴斌), Junfeng Zhu(朱军峰), Degang Xu(徐德刚), and Jianquan Yao(姚建铨)

Chin. Phys. B, 2022, 31 (**2**): 024204. DOI: 10.1088/1674-1056/ac2d20

Surface plasmon polaritons induced reduced hacking

Bakhtawar, Muhammad Haneef, and Humayun Khan

Chin. Phys. B, 2021, 30 (**6**): 064215. DOI: 10.1088/1674-1056/abd7e5

High efficiency sub-nanosecond electro-optical *Q*-switched laser operating at kilohertz repetition frequency

Xin Zhao(赵鑫), Zheng Song(宋政), Yuan-Ji Li(李渊骥), Jin-Xia Feng(冯晋霞), Kuan-Shou Zhang(张宽收)

Chin. Phys. B, 2020, 29 (**8**): 084205. DOI: 10.1088/1674-1056/ab8ac4

Reduced graphene oxide as saturable absorbers for erbium-doped passively mode-locked fiber laser

Zhen-Dong Chen(陈振东), Yong-Gang Wang(王勇刚), Lu Li(李璐), Rui-Dong Lv(吕瑞东), Liang-Lei Wei(韦良雷), Si-Cong Liu(刘思聪), Jiang Wang(王江), Xi Wang(王茜)

Chin. Phys. B, 2018, 27 (**8**): 084206. DOI: 10.1088/1674-1056/27/8/084206

2-μm mode-locked nanosecond fiber laser based on MoS_2 saturable absorber

Xiao-Fa Wang(王小发), Xiao-Ling Peng(彭晓玲), Qiu-Xia Jiang(姜秋霞), Xiao-Hui Gu(顾小辉), Jun-Hong Zhang(张俊红), Xue-Feng Mao(毛雪峰), Su-Zhen Yuan(袁素贞)

Chin. Phys. B, 2017, 26 (**11**): 114205. DOI: 10.1088/1674-1056/26/11/114205

The 266-nm ultraviolet-beam generation of all-fiberized super-large-mode-area narrow-linewidth nanosecond amplifier with tunable pulse width and repetition rate

Shun Li(李舜), Ping-Xue Li(李平雪)†, Min Yang(杨敏), Ke-Xin Yu(于可新), Yun-Chen Zhu(朱云晨), Xue-Yan Dong(董雪岩), and Chuan-Fei Yao(姚传飞)

Institute of Ultrashort Pulsed Laser and Application, Faculty of Materials and Manufacturing, Beijing University of Technology, Beijing 100124, *China*

(Received 12 June 2021; revised manuscript received 20 July 2021; accepted manuscript online 30 July 2021)

We report on a compact, stable, all-fiberized narrow-linewidth (0.045 nm) pulsed laser source emitting laser beam with a wavelength of 266 nm, and tunable pulse width and repetition rate. The system is based on all-fiberized nanosecond amplifier architecture, which consists of Yb-doped fiber preamplifiers and a super-large-mode-area Yb-doped fiber power amplifier. The fiber amplifier with a core of 50 μm is used to raise the threshold of the stimulated Brillouin scattering (SBS) effect and to obtain high output power and single pulse energy. Using lithium triborate (LBO) crystal and beta-barium borate (BBO) crystal for realizing the second-harmonic generation (SHG) and fourth-harmonic generation (FHG), we achieve 17 μJ (1.73 W) and 0.66 μJ (66 mW), respectively, at wavelengths of 532 nm and 266 nm and a repetition rate of 100 kHz with pulse width of 4 ns. This source has great potential applications in fluorescence research and solar-blind ultraviolet optical communication.

Keywords: nanosecond, all-fiber amplifier, narrow-linewidth, ultraviolet beam generation, tunable pulse width and repetition rate

PACS: 42.55.–f, 42.55.Wd, 42.65.Ky **DOI:** 10.1088/1674-1056/ac192b

1. Introduction

Nowadays, there is an increasing need for narrow-linewidth, high average power ultraviolet (UV) laser sources for high-resolution spectroscopy, remote environmental sensing, laser-induced fluorescence, semiconductor inspection, and light detection and ranging (LIDAR) applications.[1,2] Especially, the deep-UV lasers with narrow-linewidth (< 10 GHz) can improve the effect significantly for the above-mentioned applications.[3,4] So far, using narrow-linewidth solid-state lasers as fundamental frequency sources for frequency conversion, has been the most popular method to produce UV lasers.[5–14] In addition, narrow-linewidth fiber lasers are also potential fundamental frequency sources, which can provide better-quality beams, improved compactness, higher stability and efficiency.[15] Furthermore, narrow-linewidth fiber lasers are easy to achieve tunable repetition frequency and pulse width, compared with solid-state lasers.

Producing narrow-linewidth deep-UV lasers requires a fundamental frequency source with higher peak power.[16] However, the peak power of narrow-linewidth fiber lasers, related to the pulse duration of the order of ns, is relatively low for efficient frequency quadrupling. In addition, the limitation of the SBS effect is more obvious for narrow-linewidth fiber lasers.[17,18] In order to improve the peak power values of fundamental frequency sources of narrow-linewidth fiber lasers, Brooks and Teodoro used the spatially coupled photonic crystal fiber as a main power amplifier to generate an 8-GHz linewidth deep-UV laser.[3] The pulse duration was about 1 ns at 13.4 kHz, corresponding to the 265.5-nm deep-UV laser with the average power of 1.9 W. Délen *et al.*[16] employed Yb:YAG single-crystal fibers reducing the SBS limitation to obtain a 35-MHz linewidth, 257-nm-wavelength deep-UV laser, which was operated at 30 kHz with a pulse duration of 15 ns and average power of 3.2 W. Xuan *et al.*[19] presented a 2-GHz linewidth, 258-nm-wavelength deep-UV beam generated by Yb:YAG single-crystal fiber amplifier with average power of 10.5 W at a pulse repetition rate of 10 kHz. Nonetheless, these methods break the all-fiber laser structure and require a large number of space components, which greatly weakens the advantages of all-fiber lasers. Furthermore, He *et al.*[15] used an all-fiber amplifier as a fundamental frequency source to achieve a 2-W, 274-nm-wavelength deep-UV laser with a pulse width of 1.8 ns and a repetition rate of 200 kHz. Kumar *et al.*[20] demonstrated a deep-UV laser with 1.8 W in power, 17 ps in pulse width, 266 nm in wavelength at a high repetition rate of 79.5 MHz generated by a mode-locked Yb-fiber laser. However, the spectral width values of the above-mentioned two lasers are 0.16 nm and 1.4 nm respectively, which reduces the spectral resolution of narrow-linewidth laser in practical applications. In the field of solar-blind UV communication, the narrow-linewidth laser will further increase the communication speed due to its good time coherence. The application of narrow-linewidth lasers in the

†Corresponding author. E-mail: pxli@bjut.edu.cn

© 2022 Chinese Physical Society and IOP Publishing Ltd

field of solar-blind UV communication will become the inevitable trend of the development of coherent communication technology in the future. For the narrow-linewidth fiber lasers, the spectral width of the fiber laser needs to be strictly controlled due to the fiber having wide gain spectrum. Therefore, it is valuable to utilize the inherent advantages of all-fiber laser, especially for its relatively simple and compact configuration to produce a narrow-linewidth (< 10 GHz) deep-UV all-fiber laser.

On the other hand, lasers with tunable pulse width and repetition frequency show excellent application advantages, which is particularly obvious around the wavelength of 1 μm[21–23] while rarely reported in deep-UV wavelength range. For example, characterized by tunable pulse width, deep-UV lasers can affect the geometric accuracy and surface quality of the submicron structures.[24] The deep-UV lasers with suitable repetition frequency will directly improve the cutting quality and processing efficiency.[25] Moreover, the deep-UV lasers with tunable pulse width have the great requirements of applications, especially, in wireless solar-blind UV communication, of which the parameters are significantly affected by pulse width, such as receiver elevation angle, receiver field-of view, and communication distance.[26] However, the pulse width can be easily stretched in the practical application of solar-blind UV communication due to the multiple-scattering interaction.[27] Therefore, the deep-UV lasers with tunable pulse width can improve the quality of communication.

The aim of the present investigation is to integrate a compact deep-UV laser with tunable pulse width for wireless solar-blind UV communication. Compared with the commonly used excimer lasers, the UV light-emitting-diodes (LEDs)[28] and UV lamps, our miniaturized narrow-linewidth deep-UV laser has huge potential applications in reducing bit error rate and improving sensitivity of UV communication. In this paper, we report on a compact, stable, all-fiberized narrow-linewidth pulsed laser source emitting laser beam with a wavelength of 266 nm. The system is based on an all-fiberized nanosecond amplifier architecture and nonlinear frequency conversion stages. The nanosecond amplifier generates 4.15-ns pulses at $\lambda \sim 1064$ nm with average output power of 13.8 W, corresponding to the spectral bandwidth of 0.045 nm. The fourth-harmonic generation (FHG) is achieved by using an 18-mm lithium triborate (LBO) crystal to generate 532-nm second harmonic (SH) with average power of 1.73 W, followed by a 7-mm beta-barium borate (BBO) crystal to generate 266-nm fourth harmonic (FH) with average power of 66 mW at a repetition rate of 100 kHz with a pulse width of 4 ns. The corresponding conversion efficiency of the SHG and the FHG are 12.5% and 3.8%, respectively.

2. Experimental setup

The fundamental frequency source, which is an all-fiberized narrow-linewidth (0.045 nm) Yb-doped nanosecond laser amplifier system, was composed of a laser diode seed source, Yb-doped fiber preamplifiers and a commercial 50-μm-core Yb-doped-diameter fiber amplifier as shown in Fig. 1. A commercial distributed feedback laser diode was used as a seed source. Using the intracavity optical feedback method, the Bragg grating was distributed in the entire resonant cavity for mode selection to produce narrow-linewidth lasers. By adopting the method of high-doped, short-length and super-large-mode-area gain fibers for power amplifications, the SBS threshold could be increased and the nonlinear effects could be reduced. This is an effective method to generate high-power narrow-linewidth lasers. The basic narrow-linewidth fiber amplifier architecture followed our previous work.[29] When the pulse duration and the repetition frequency of the laser amplifier system were set to be 4 ns and 100 kHz, respectively, the laser amplifier delivered 13.8-W average power corresponding to the pulse energy of 138 μJ centered at 1064.1 nm as shown in Fig. 2. The typical spectrum (0.02-nm resolution) from the fundamental frequency source is shown in Fig. 2(a), which has a 0.045-nm (11.9 GHz) full width at half-maximum (FWHM) centered at 1064.1 nm. The self-phase modulation (SPM) effect in fiber is a nonlinear effect that is most likely to broaden the spectral line width. In addition, the wider gain spectrum in the fiber can easily lead to spectral broadening. In our experiment, we did not detect nonlinear effects, nor obvious spectral broadening due to the application of short length, highly doped and super-large-mode-area gain fibers to power amplifications, which was precisely the advantage of this work. The result, show that the spectral line width of the seed source and the amplifier are 0.041 nm and 0.045 nm, respectively. This means that there was no obviously spectral broadening in an average power range from tens of mW to 13 W. Generally, there is a strong soliton effect in the negative dispersion region of the fiber, which is investigated in detail in Refs. [30–32]. However, there was found no soliton effect in our narrow-linewidth laser. This was because the wavelength of our laser is 1064 nm which is located in the positive dispersion region. Figure 2(b) displays the temporal profile of the fundamental frequency laser pulses, measured by a digital oscilloscope (LyCroy, sampling rate: 13 GHz), showing the pulse duration of 4.15 ns. The inset in Fig. 2(b) indicates the pulse sequence. The maximum output power of the fundamental frequency source is 13.8 W (see Fig. 2(c)). Figure 2(d) shows the beam quality M^2 values of 2.56 (horizontal) and 3.17 (vertical), measured by a laser beam analyzer (M^2-200, Ophir-Spiricon). The whole laser system was composed of non-polarization maintaining fibers.

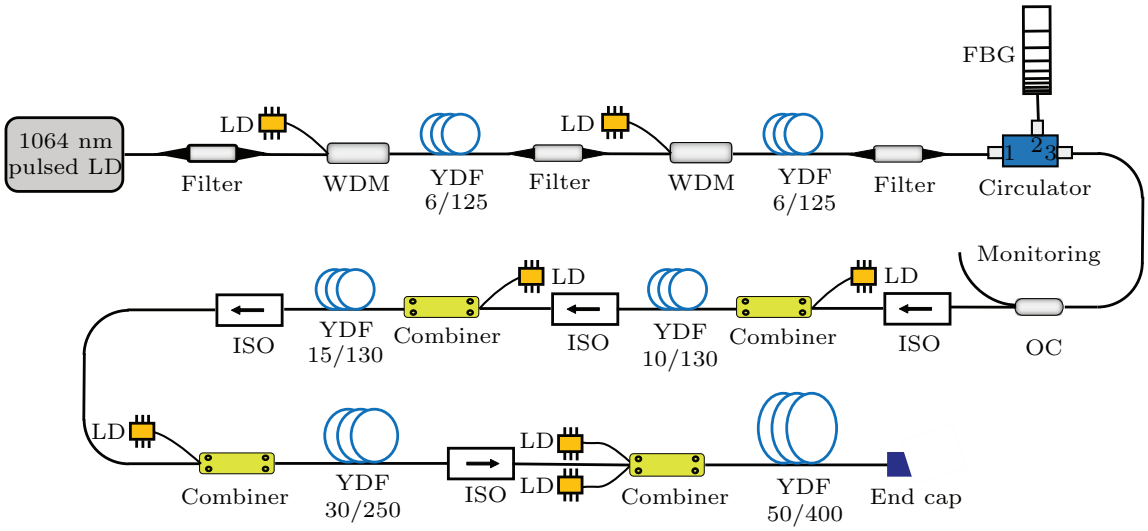


Fig. 1. Schematic diagram of narrow-linewidth nanosecond all-fiber amplifier system.

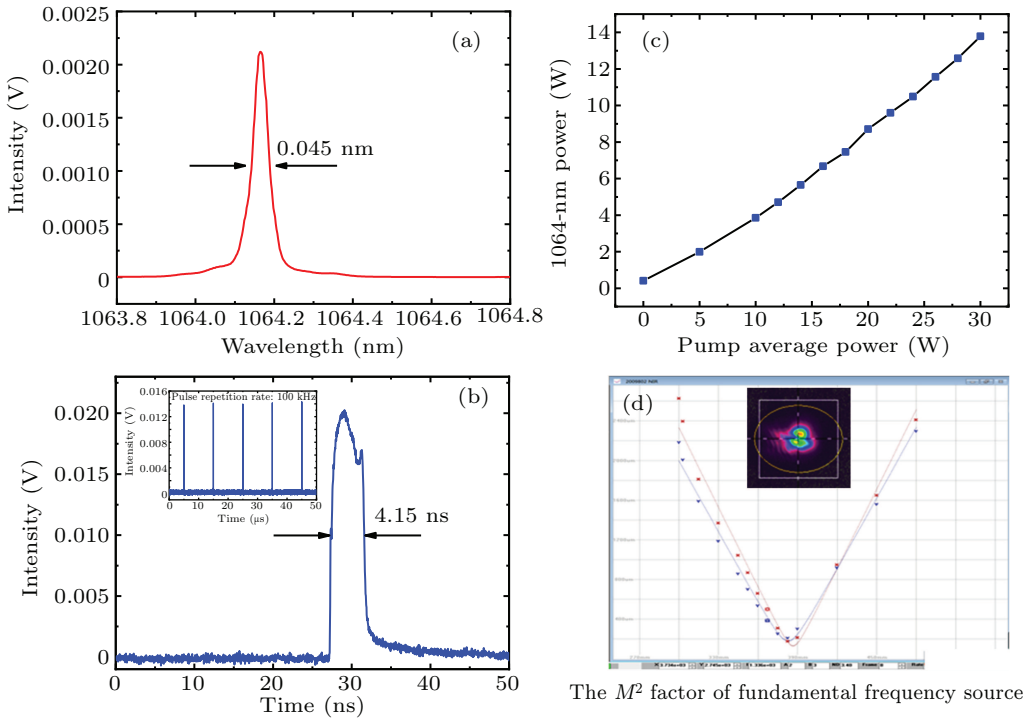


Fig. 2. (a) Optical spectrum; (b) single pulse shape at output power of 13.8 W, with inset showing pulse sequence; (c) 1064-nm average power; and (d) M^2 factor of fundamental frequency source.

Figure 3 shows the optical layout of the SHG module and the FHG module from the narrow-linewidth all-fiber nanosecond laser amplifier system. We used an LBO crystal for SHG because of its excellent properties, such as high damage threshold, small walk-off angle and high nonlinear coefficient. Furthermore, the method of critical phase matching (CPM) of LBO working at room temperature, is conducive to the integration of deep-UV lasers. The crystal was Y–Z cut ($\theta = 20.9°$) with $\phi = 90°$ for type-II phase-matched SHG kept at 24.5 °C. The temperature of the LBO crystal was precisely controlled by a thermo electric cooler (TEC) controller with the controlling precision of ±0.1 °C. The crystal dimensions were 4 mm×4 mm×18 mm and the two crystal ends were both antireflection (AR) coated at wavelengths of 1064 nm and 532 nm. The collimated non-polarization maintaining pump beam passed through a combination of a quarter-wave plate (QWP), half-wave plate (HWP), and polarizing beam splitter (PBS) cube to obtain the linearly polarized laser with relatively high power. Subsequently, the second HWP was used to obtain the required polarization state for phase matching in the frequency conversion crystal. Then the spot diameter of the polarized laser was focused into 0.6 mm through a lens with $f = 75$ mm. After the SHG inside the LBO crystal, the residual pump beam was split from the SH beam by a 1064-nm/532-nm dichroic mirror (DM) which reflected the laser of 532 nm and transmitted the laser of 1064 nm.

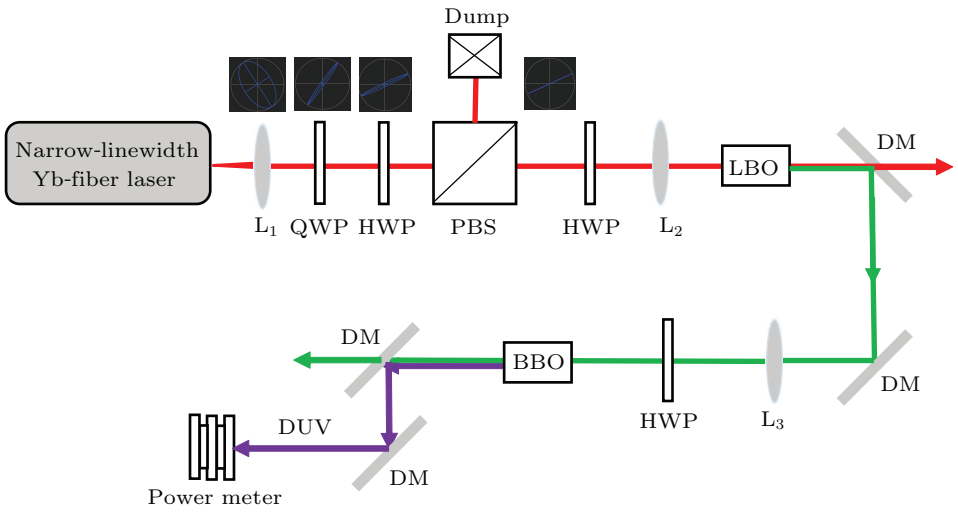


Fig. 3. Schematic diagram of Yb-fiber-amplifier-based narrow-linewidth nanosecond deep-UV laser. L: lens; QWP: quarter-wave plate; HWP: half-wave plate; PBS: polarizing beam splitter; and DM: dichroic mirror.

The FHG from 532 nm to 266 nm was achieved by a BBO crystal (4 mm×4 mm×7 mm, $\theta = 45.7°$, $\phi = 0°$, type-I phase-matching ($o + o \rightarrow e$)), which is more commonly available and less hygroscopic than the other UV nonlinear crystals such as $CsLiB_6O_{10}$ (CLBO) and KH_2PO_4 (KDP). The crystal coated with ARs of 532 nm and 266 nm on both sides was mounted in a three-dimensional adjustment frame for optimizing the phase matching conditions. The 532-nm pump beam generated by SHG in LBO was coupled into the BBO crystal by a focusing lens with $f = 60$ mm and an HWP for the optimization of the polarization state. After FHG inside the BBO crystal, the residual 532-nm pump beam was split from the FH beam by a DM which reflects the laser of 266 nm and transmits the laser of 532 nm. In the entire experimental device, each of the spherical mirrors caused about 5% of power loss because they were not coated with AR coatings.

3. Experimental results and discussion

The maximum fundamental frequency laser of 13.8 W (138 μJ) is achieved from the all-fiberized amplifier at a repetition rate of 100 kHz with a pulse width of 4 ns. Furthermore, the repetition frequency and pulse width can be continuously adjusted in a range of 5 kHz–100 kHz and from 4 ns to 8 ns, respectively. For the SHG setup, we initially perform focusing optimization of SH beam waist radius in the LBO crystal by using several lenses, L_2, with radius of curvature of 25 mm, 75 mm, 150 mm respectively. The results indicate that the 75-mm focusing lens shows a compromise between the beam waist radius and the frequency doubling distance in the LBO crystal, so it corresponds to a highest frequency conversion efficiency in the three focusing lenses. Figures 4(a) and 4(b) show the dependence of the SH power and the conversion efficiency on pump average power, respectively. By optimizing the angle of the LBO crystal, 1.73-W, 17-μJ SH pulses are obtained, with a corresponding conversion efficiency being 12.5%. The main reasons for the low frequency conversion efficiency are as follows: owing to the elliptical polarization characteristics, about half of the fundamental frequency laser power is lost before reaching the LBO crystal. As shown in Fig. 3, we have measured the polarization states of the fundamental frequency laser behind L1, QWP, HWP, and PBS respectively. It can be observed from the figure that the fundamental frequency laser is initially elliptically polarized light. The laser is then adjusted into a linearly polarized laser as much as possible by using a QWP. After that, the polarization direction of the fundamental frequency laser is adjusted to match the polarization direction of the laser passing through the PBS by using an HWP. It should be noted that the purpose of using a QWP is only to increase the laser power through the PBS as much as possible. If a polarization-maintaining (PM) laser is used as the fundamental frequency source, the conversion efficiency of the SHG will be further improved. In addition, the imperfect M^2 values of the fundamental frequency laser limit the improvement of frequency conversion efficiency. The spectrum of the SH wave centered at 532 nm is measured with an Ocean HR4000CG-UV-NIR spectrometer (resolution of 0.75 nm at 500 nm), and the results are shown in Fig. 4(c). Figure 4(d) shows the pulse duration is 4.12 ns at an output power of 1.73 W. The pump intensity on LBO crystal is 4.7 MW/cm^2 far below the damage threshold of LBO crystal (15 GW/cm^2).

The maximal FH power generated in our experiments is 66 mW (0.66 μJ), which is achieved by using a collimated pump beam with a beam diameter of 0.9 mm and pump power of 1.73 W. The dependence of the deep-UV average power and conversion efficiency on green average power are shown

in Figs. 5(a) and 5(b), respectively. The maximum conversion efficiency is about 3.8% and occurs at pump power of 1.73 W. The narrow-linewidth lasers should have a high frequency conversion efficiency. However, after optimizing the parameters of the FHG experiment, including the angle of BBO crystal, focal length of lens at the position of the beam waist in the crystal, the frequency conversion efficiency is not further improved. He *et al.*[15] also obtained a low conversion efficiency at the pump power of 1.7 W under the conditions similar to our experimental conditions. The conversion efficiency η can be obtained from the following equation:

$$\eta = \frac{8\omega^2 d^2 L^2}{\varepsilon_0 n_{2\omega} n_\omega^2 c^3} \frac{P_\omega(0)}{S} \mathrm{sinc}^2\left(\frac{\Delta kL}{2}\right),$$

where n_ω and $n_{2\omega}$ are the refractive index of the fundamental frequency laser and the frequency-doubled laser in the crystal, respectively; ε_0 and c are the dielectric constant and the speed of light in vacuum, respectively; L, d, and S are crystal length, frequency doubling coefficient, and cross-sectional area, respectively; $P_\omega(0)$ is fundamental frequency laser power. It can be seen from the above formula that η is proportional to $P_\omega(0)$, d^2, and L^2, and inversely proportional to S. In our experiment, d^2, L^2, and S are difficult to further optimize while $P_\omega(0)$ is the most effective way to further increase the conversion efficiency. In this work, the pump peak-power intensity on BBO crystal is only 518 kW/cm^2, which is not sufficient for efficient conversion efficiency. We predict that when we use a PM laser and further increase the fundamental frequency laser power to 30 W, the frequency conversion efficiency can be improved by more than 16%. Figures 5(c) and 5(d) show the spectrum and the single pulse shape of deep-UV pulses with 66-mW average power. The deep-UV spectrum shows the center wavelength of the laser is 266 nm. The inset in Fig. 5(d) indicates the pulse sequence. The small pulse peaks in the pulse waveforms in Figs. 2(b), 4(d), and 5(d) appear in the seed source of narrow-linewidth distributed feedback LD. The grating is made in the active area, it is easy to introduce defects, which leads to the spontaneous emission effect.[33] This is probably the reason for the small pulse peaks in the pulse waveform.

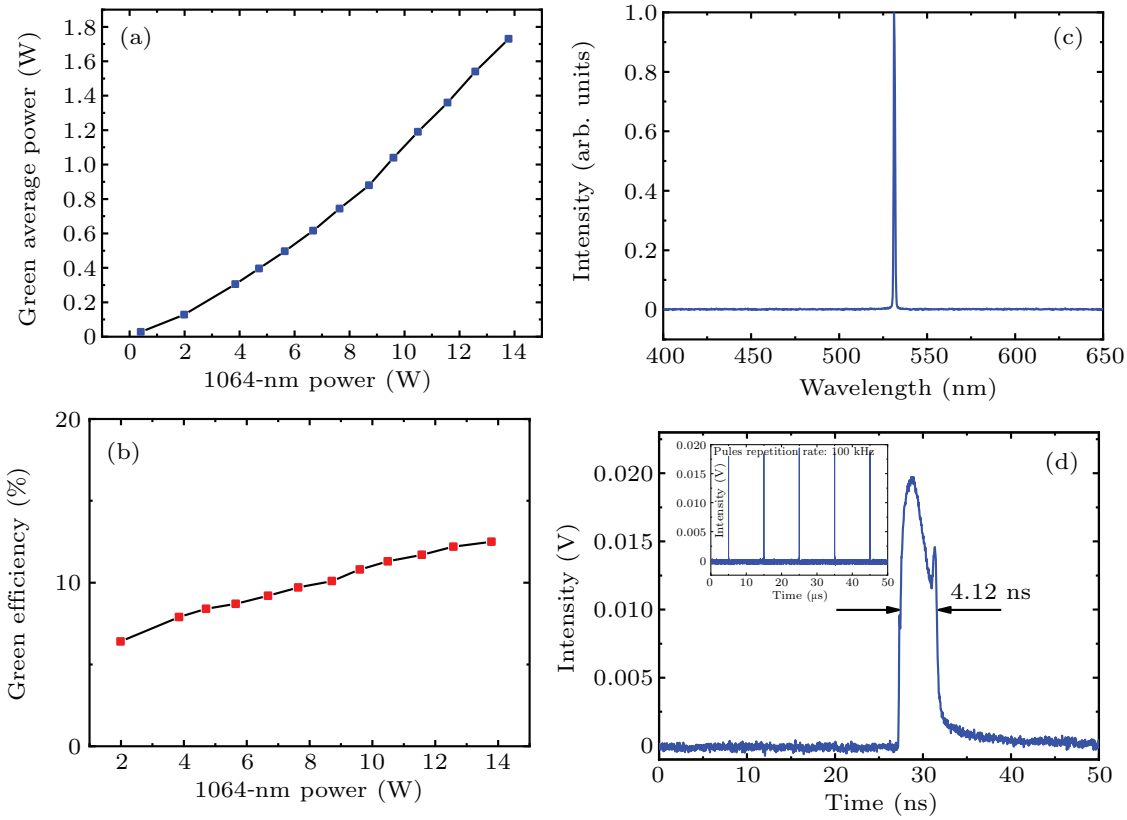


Fig. 4. (a) Green average power and (b) conversion efficiency *versus* pump average power. (c) Green spectrum and (d) single pulse shape at 1.73 W average power with inset indicating the pulse sequence at output power of 1.73 W.

Finally, we obtain 25-mW and 5-mW 266-nm deep-UV laser output, corresponding to the 50-kHz repetition frequency, 4-ns pulse width and 100-kHz repetition frequency and 8-ns pulse width respectively. The obtained results are summarized in Table 1. In practical applications, the repetition frequency and pulse width of the laser can be conveniently tuned in a range of 50 kHz–100 kHz and 4 ns–8 ns, which can achieve an optimal application effect. Since there is no saturation of UV power nor conversion efficiency, next step we will use an all-fiber PM fundamental frequency source with higher output power and better beam quality to further optimize the conversion efficiency of the deep-UV laser.

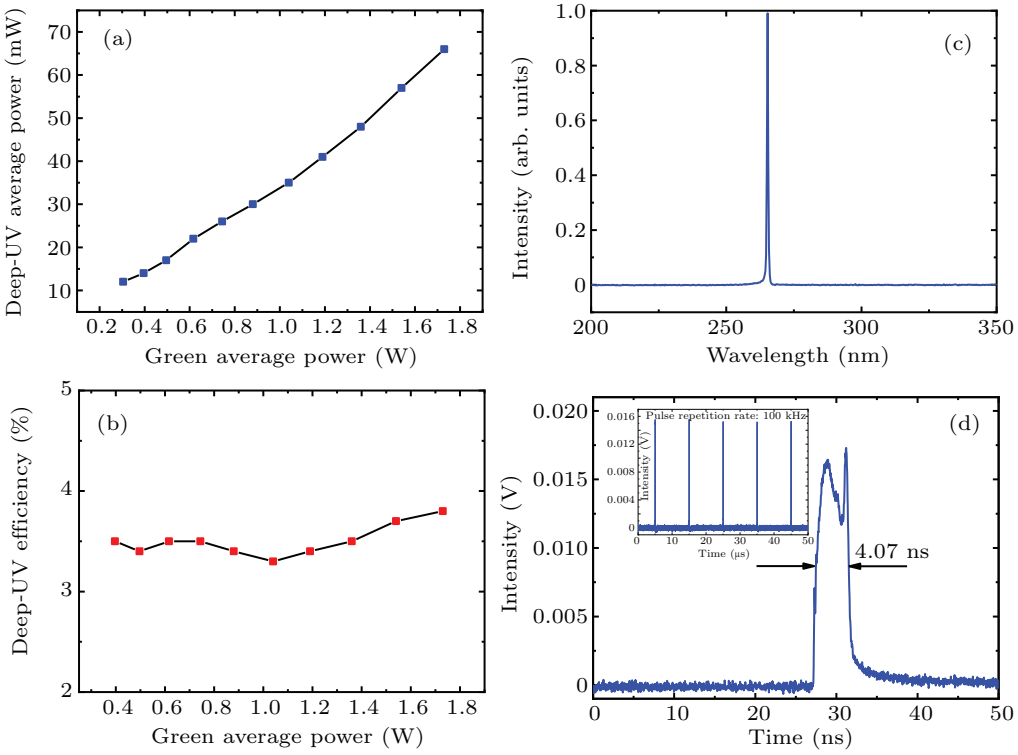


Fig. 5. Plot of (a) deep-UV average power and (b) conversion efficiency *versus* green average power. Plot of (c) deep-UV spectrum and (d) single pulse shape at 66-mW average power, with the inset showing pulse sequence at output power of 66 mW.

Table 1. Summary of harmonic generation results.

Repetition rate (kHz)	Pulse duration (ns)	Average power 1064 nm (W)	Average power 532 nm (W)	Average power 266 nm (mW)	SHG efficiency from 1064 nm (%)	FHG efficiency from 532 nm (%)
100	4	13.8	1.73	66	12.5	3.8
50	4	4.7	0.543	25	11.5	4.6
100	8	3.0	0.240	5	8	2

4. Conclusions

In this work, we report on a compact, stable, all-fiberized narrow-linewidth pulsed laser source emitting a laser with a wavelength of 266 nm, tunable pulse width and repetition rate. The system is based on an all-fiberized nanosecond amplifier architecture and nonlinear frequency conversion stages. Using LBO crystal and BBO crystal for the SHG and FHG, respectively, we achieve 17 μJ (1.73 W) and 0.66 μJ (66 mW), respectively, at wavelengths of 532 nm and 266 nm with a repetition rate of 100 kHz and pulse width of 4 ns. The corresponding conversion efficiency of the SHG and the FHG are 12.5% and 3.8%, respectively. We will use a higher power PM all-fiber narrow-linewidth laser amplifier and continue to optimize the conversion efficiency of the deep-UV laser in the future.

Acknowledgements

Project supported by the Key Program of Beijing Municipal Natural Science Foundation, China (Grant No. KZ201910005006), the National Nature Science Foundation of China (Grant No. 62005004), the Natural Science Foundation of Beijing Municipality, China (Grant No. 4204091), and the National Science Foundation for Postdoctor Scientists of China (Grant No. 212423).

References

[1] Case A T, Tan D, Stickel R E and Mastromarino J 2006 *Appl. Opt.* **45** 2306
[2] Ostermeyer M, Kappe P, Menzel R and Wulfmeyer V 2005 *Appl. Opt.* **44** 582
[3] Christopher D B and Fabio Di Teodoro 2007 *Opt. Commun.* **280** 040
[4] Zhang X, Yang F, Feng Z T, Zhao J J, Wei F, Cai H W and Qu R H 2019 *Chin. Phys. B* **28** 074209
[5] Kojima T, Konno S, Fujikawa S, Yasui K and Okada Y 2000 *Opt. Lett.* **25** 058
[6] Wang G L, Geng A, Bo Y, Li H Q, Sun Z P, Bi Y, Cui D F, Xu Z Y, Yuan X, Wang X Q, Shen G Q and Shen D Z 2006 *Opt. Commun.* **259** 061
[7] Liu Q, Yan X P, Fu X, Gong M and Wang D S 2009 *Laser Phys. Lett.* **6** 10122
[8] Liu Q, Yan X P, Gong M L, Liu H, Zhang G and Ye N 2011 *Opt. Lett.* **36** 2653
[9] Wang L R, Wang G L, Zhang X, Liu L J and Chen C T 2012 *Chin. Phys. Lett.* **29** 064203
[10] Wang L R, Zhai N X, Liu L J, Wang X Y, Wang G L, Zhu Y and Chen C T 2014 *Opt. Express* **22** 027086

[11] Goldberg L, Cole B, McIntosh C, King V, Hays A D and Chinn S R 2016 *Opt. Express* **24** 017397

[12] Hong H L, Liu Q, Huang L and Gong M L 2013 *Opt. Express* **21** 7285

[13] Nikitin D G, Byalkovskiy O A, Vershinin O I, Puyu P V and Tyrtyshnyy V A 2016 *Opt. Lett.* **41** 1660

[14] Yan X, Liu Q, Chen H, Fu X, Gong M and Wang D 2010 *Laser Phys. Lett.* **7** 4131

[15] He J, Lin D, Xu L, Beresna M, Zervas M N, Alam S U and Brambilla G 2018 *Opt. Express* **26** 6554

[16] Delen X, Deyra L, Benoit A, Hanna M, Balembois F, Cocquelin B, Sangla D, Salin F, Didierjean J and Georges P 2013 *Opt. Lett.* **38** 995

[17] Wellmann F, Steinke M, Meylahn F, Bode N, Willke B, Overmeyer L, Neumann J and Kracht D 2019 *Opt. Express* **27** 028523

[18] Wang X L, Zhou P, Leng J Y, Du W B and Xu X J 2013 *Chin. Phys. B* **22** 044205

[19] Xuan H W, Qu C, Ito S and Kobayashi Y 2017 *Opt. Lett.* **42** 3133

[20] Kumar S C, Casals J C, Bautista E S, Devi K and Ebrahim Z M 2015 *Opt. Lett.* **40** 2397

[21] Cui Y L, Tang N, Zhou Z Y, Li Z X and Wang Z F 2019 *Opt. Fiber Technol.* **52** 101938

[22] Dilley C E, Stephen M A and Savage-Leuchs M P 2007 *Opt. Express* **15** 14389

[23] Zhang W, Wei Z, Wang Y B and Jin G Y 2016 *Chin. Phys. Lett.* **33** 014205

[24] Simon P and Ihlemann J 1997 *Appl. Surf. Sci.* **96** 00615

[25] Chen T C and Darling R B 2005 *Journal of Materials Processing Technology* **169** 214

[26] Chen G, Xu Z and Sadler B M 2010 *Opt. Express* **18** 010500

[27] Zhang K J, Liu L, Zeng Q W, Gao T C, Hu S and Chen M 2019 *Acta Phys. Sin.* **68** 194207 (in Chinese)

[28] Shatalov M, Zhang J P, Chitnis A S, Adivarahan V and Khan M A 2002 *IEEE* **8** 999185

[29] Yang M, Li P X, Wang D X, Yu K X, Dong X Y, Wang T T, Yao C F and Yang W X 2020 *Chin. Phys. B* **29** 114206

[30] Guo B, Wang S H, Wu Z X, Wang Z X, Wang H D, Huang H, Zhang F, Ge Y Q and Zhang H 2018 *Opt. Express* **26** 22750

[31] Song Y F, Wang Z H, Wang C, Panajotov K and Zhang H 2020 *Appl. Phys. Rev.* **2** 024001

[32] Song Y F, Wang Z H, Wang C, Panajotov K and Zhang H 2020 *Adv. Photon* **2** 024001

[33] Robadey J, Gourgon C, Gaud E, *et al.* 1999 *Electron. Lett.* **35** 2119